Control surface wettability with nanoparticles from phase-change materials

G. H. ten Brink, P. J. van het Hof, B. Chen, M. Sedighi, B. J. Kooi, and G. Palasantzas

Citation: Appl. Phys. Lett. **109**, 234102 (2016); doi: 10.1063/1.4971773
View online: http://dx.doi.org/10.1063/1.4971773
View Table of Contents: http://aip.scitation.org/toc/apl/109/23
Published by the American Institute of Physics

Control surface wettability with nanoparticles from phase-change materials

G. H. ten Brink, P. J. van het Hof, B. Chen, M. Sedighi, B. J. Kooi, and G. Palasantzas[a)]
Zernike Institute for Advanced Materials, University of Groningen, Nijenborgh 4, 9747 AG Groningen, The Netherlands

(Received 18 October 2016; accepted 22 November 2016; published online 6 December 2016)

The wetting state of surfaces can be controlled physically from the highly hydrophobic to hydrophilic states using the amorphous-to-crystalline phase transition of $Ge_2Sb_2Te_5$ (GST) nanoparticles as surfactant. Indeed, contact angle measurements show that by increasing the surface coverage of the amorphous nanoparticles the contact angle increases to high values $\sim 140°$, close to the superhydrophobic limit. However, for crystallized nanoparticle assemblies after thermal annealing, the contact angle decreases down to $\sim 40°$ (significantly lower than that of the bare substrate) leading to an increased hydrophilicity. Moreover, the wettability changes are also manifested on the capillary adhesion forces by being stronger for the crystallized GST state. *Published by AIP Publishing*. [http://dx.doi.org/10.1063/1.4971773]

Although a topic of more than 200 years old, wetting of liquids on solid surfaces attracts nowadays relentless attention from the fundamental and application point of view.[1–9] A few examples include self-cleaning, anti-icing, adhesion of material surfaces, stiction issues in micro-electromechanical systems (MEMS), capillarity, reduced fluid drug in micro/nanofluidic systems, etc. Moreover, trapping of water drops by modification of surface wettability plays important role for the efficiency of drop condensation from vapor in heat exchangers and fog harvesters.[5–9] The surface wettability is measured by the contact angle (CA) between a water droplet and the supporting surface. A surface with $CA < 90°$ is termed as hydrophilic, while one with $CA > 90°$ is termed as hydrophobic.[1,2] Superhydrophobic surfaces with $CA \sim 150°$ have also attracted strong interest[1,2] inspired by many examples in nature (e.g., duck feathers, butterfly wings, lotus plant, etc.).[10–15]

Controlling surface wettability by surface roughening and chemical modification is a topic of intense research area.[1–9] The contact angle CA_f for a flat surface is given by the Young equation $\cos CA_f = (\gamma_{sg} - \gamma_{sl})/\gamma_{lg}$[1,2] with γ_{sg}, γ_{sl} and γ_{lg} the solid-gas, solid-liquid and liquid-gas interface energies, respectively. For rough surfaces, the Wenzel (W) model predicts that a hydrophilic/hydrophobic surface would be more hydrophilic/hydrophobic with surface roughening assuming complete contact of the liquid with the surface.[16] Nevertheless, droplets on a rough surface are not expected to wet deep surface crevices, leaving air pockets in between crevices and forming the Cassie-Baxter (CB) state.[17] During CB → W transitions, thermodynamically unstable air pockets allow liquid to nucleate into crevices.[18]

Processes to form hydrophobic surfaces involve combinations of surface roughening with the alteration of surface chemistry using low surface energy materials to mimic the structure of the lotus leaf or butterfly wings that show strong hydrophobicity.[1–4] Other methods used random and deterministic structured microscale roughness.[2,19–22] The latter, resembling grid of pillars or nail heads, have attracted interest to create superhydrophobic and possibly omniphobic surfaces.[2,23–25] Nanometer-size textures could facilitate more resilient coatings due to nanoscale geometry and confinement effects.[22] Thermodynamically, a hydrophobic rough surface can be formed from hydrophilic material if the roughness is multivalued.[26] Near superhydrophobicity and trapping of water droplets were also demonstrated for surfaces coated by the Cu nanoparticles (NPs) produced by high pressure magnetron sputtering.[27]

Although micro/nanoscale surface roughness can lead to enhanced hydrophobicity, the physical change of surface wettability between hydrophilic and, even, superhydrophobic states by switching the phase state of materials, without material composition changes and additional surface micro/nano-structuring, is highly nontrivial. It will be shown here, as a *concept-of-proof*, that this can be achieved for surfaces covered by NPs derived from phase-change materials (PCMs)[28,29] when they undergo reversible amorphous (A)-to-crystalline (C) phase transitions. In fact, PCMs are not only renowned for their use as active media in rewritable optical disks (i.e., CD, DVD, and Blu-Ray Disks) using reversible A-C phase transitions,[28,29] but they are also promising to provide the required reversible modification of the dielectric response, leading to a significant Casimir force contrast.[30,31]

Here, the $Ge_2Sb_2Te_5$ (GST) NPs[32,33] were produced using high pressure plasma sputtering in a modified *Mantis Nanogen 50* system (see in supplementary material Figs. 1S and 2S).[33,34] The GST NPs were deposited on highly oriented pyrolytic graphite (HOPG) surfaces (approaching hydrophobic behaviour) that have significant $CA \sim 70°$ in order to illustrate more clearly the formation of distinct hydrophobic/hydrophilic states. Initially, the NPs were deposited using a low discharge current ~ 0.1 A to ensure that they were in the amorphous state.[32] Furthermore, the amorphous NP assemblies on HOPG were crystallized by ex-situ annealing for 10 min on a hot plate at a temperature of $\sim 120\,°C$.[32] The homogeneity and roughness of the surfaces were assessed with a Bruker atomic force microscope

[a)]Author to whom correspondence should be addressed. Electronic mail: g.palasantzas@rug.nl

(AFM, Multimode 8; see Fig. 1) in combination with scanning electron microscopy (SEM; see in supplementary material Fig. 3S). The samples were all made using the same settings to ensure that the NPs were of comparable size (~10%) and only the deposition time was varied between samples to obtain varying degrees of NP coverages on the sample surfaces. Moreover, transmission electron microscope (TEM) samples (see in supplementary material Figs. 4S) underwent deposition simultaneously as those for the contact angle measurements, and they were analyzed in a JEOL 2010 TEM to enable calculation of the surface coverage and measurement of the NP size distribution with the Image-Pro Plus v4.5 software.[33]

The AFM images of the samples were taken over areas 3×3–$5 \times 5\ \mu m^2$ to calculate the root mean squared (RMS≡w) roughness. Height-height correlation difference function analysis, $g(x) = \langle [h(x)-h(0)]^2 \rangle$ vs. lateral scale x, with $\langle \ldots \rangle$ indicating statistical average, from the topography data (Fig. 1) yielded all necessary roughness parameters. Besides w, one obtains from g(x) the lateral roughness correlation length ξ and the roughness exponent H ($0 < H < 1$), for which $g(x) \approx \rho^2 x^{2H}$ for $x \ll \xi$, to estimate the average local surface slope $\rho(\approx w/\xi^H)$[35,36] for roughness exponents H significantly lower than 1 (see in supplementary material Fig. 5S). The obtained average surface local slope $\varphi = \tan^{-1}\rho$ ($\rho \approx w/\xi^H$)[36] was rather significant, indicating the formation of a steep nanoscale topology (e.g., $\varphi \approx 40°$ for the amorphous GST NPs in Fig. 1(a)). Although the AFM morphologies in Fig. 1 appear similar, the amorphous surface has particles more distinct and uniform in size (without any significant coalescence as TEM analysis indicated[32]) that is inherent to soft impact deposition of NPs leading to porous assemblies. However, for the crystalline surface, some coalescences occur during annealing leading to a larger variation of grain sizes and lower porosity but rougher than the amorphous surface (as also the z-scales indicate). Notably, during the initial stages of NP deposition, we observed preferential decoration of surface step edges (inset Fig. 1(a)) due to stronger van der Waals forces on surface steps than on planar parts of the HOPG surface.[37,38]

To measure the wetting state of samples, the contact angle measurements were performed using a Dataphysics OCA25 system (see Fig. 2 and in supplementary material Fig. 6S). An automated syringe dropped ~2 μl droplets of pure water

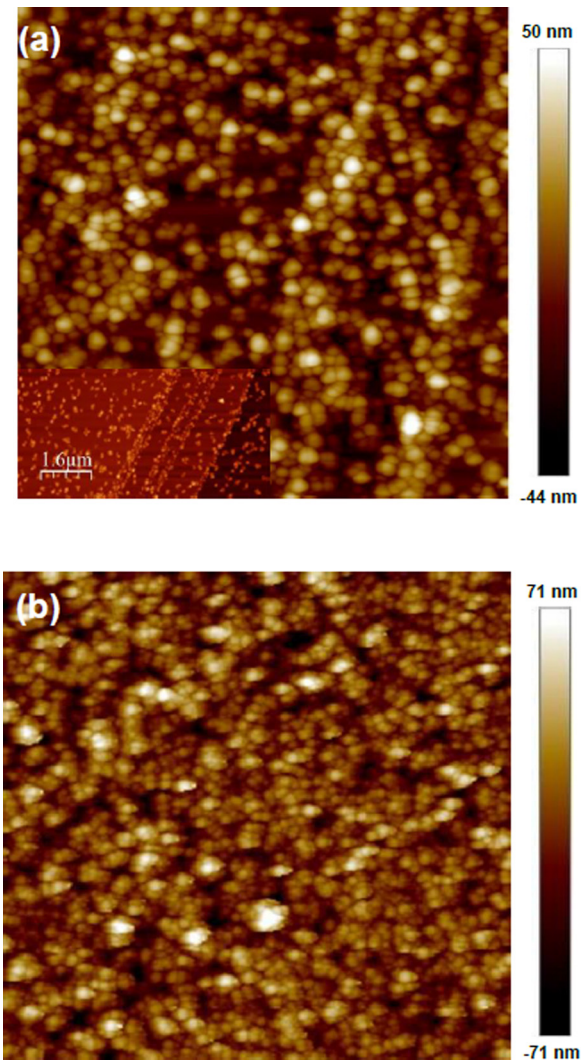

FIG. 1. (a) AFM topography of amorphous NPs. The inset shows the preferential decoration of NPs at HOPG step edges during initial deposition stages. (b) AFM topography of crystallized NP assemblies. The topology indicates partial fusion of NPs yielding a more compact granular structure with reduced porosity. In both cases, the scan area was $3 \times 3\ \mu m^2$.

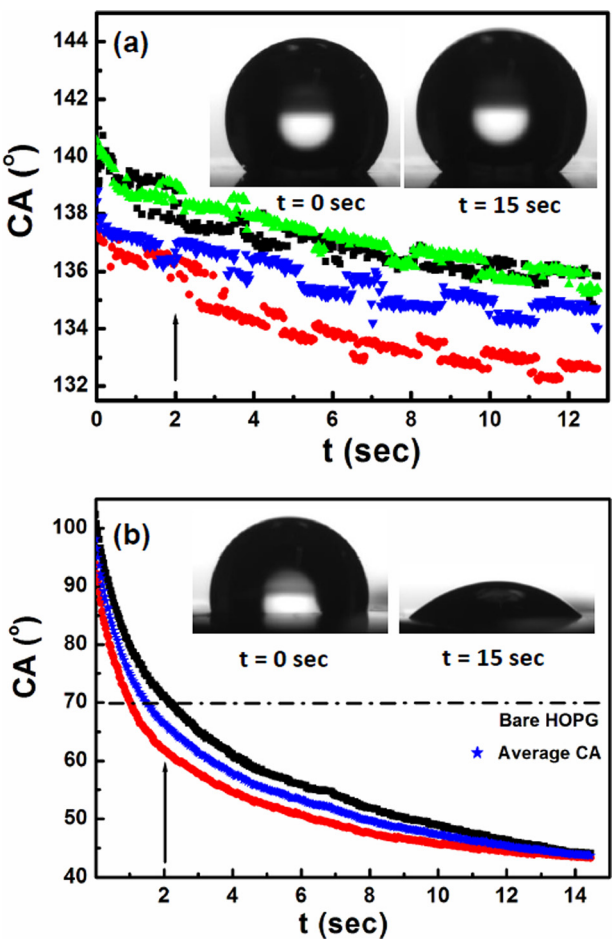

FIG. 2. (a) Contact angle (CA) vs. relaxation time (t) for amorphous GST NPs with data taken from different locations on the sample surface. (b) Contact angle (CA) vs. relaxation time (t) for crystalline GST NPs with data taken at two different locations on the sample surface (for illustration purposes). The insets show in both cases the contact angle images of the initial (t = 0 s) and final states (t = 15 s) of the water droplets (see also in supplementary material Fig. 6S).

(MilliQ) on the sample, where a camera recorded the pictures over a period of several seconds. The drop shape is analyzed based on the shape of an ideal sessile drop, the surface curvature of which results only from the force equilibrium between surface tension and weight. The values of the contact angle were obtained via a fit using the Young-Laplace (YL) equation based on the shape analysis of a complete drop and also compared to the results obtained from the geometrical CA analysis.[39,40] For every sample, the CA measurements were repeated for several drops on different sample areas.

Figures 2 and 3 show the temporal evolution of the CA on HOPG coated with amorphous and crystallized GST NPs of high coverage (>80% to obtain high CA values for the amorphous NPs, as we have shown in our previous studies[27]), respectively. For the as-deposited amorphous NPs in Fig. 2(a), the CA after a transient relaxation ~2 s still preserves a large value CA > 132° that indicates strong hydrophobicity. Indeed, the CA is almost twice that of the bare HOPG surface (CA ~ 70°), and it is comparable to those measured for high coverage of Cu NPs.[27] However, for the crystallized GST (Fig. 2(b)) after annealing, the CA after a rapid drop within ~2 s approaches values less than that of the bare HOPG surface and dramatically reduces to a hydrophilic state with CA ~ 40°, which is comparable to the hydrophilic SiO_x surfaces.[27]

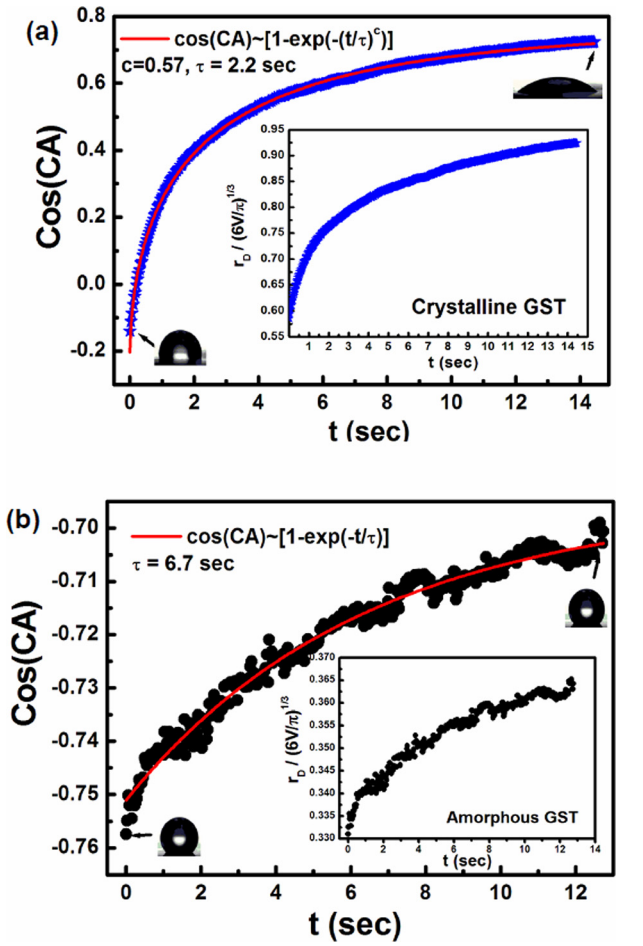

FIG. 3. (a) cos(CA) vs. relaxation time t for crystalline GST NPs using the averaged data from Fig. 2 with the corresponding fit curve. The inset shows the temporal dependence of the droplet radius. (b) Similar plots as in (a) for crystallized GST NPs.

Further analysis of the relaxation dynamics of CA for the crystalline GST was performed in Fig. 3(a), using the averaged data of Fig. 2(a). Since in the past the kinetics of wetting and spreading have been described via a single exponential behaviour $\cos(CA) \sim [1 - \exp(-t/\tau)]$,[41,42] we fitted our data for cos(CA) using the more general form $\cos(CA) = \cos(CA|_{t=0}) + A[1 - \exp(-(t/\tau)^c)]$. In our case, we obtained the exponent $c = 0.57$, which is smaller than the single exponential case ($c = 1$), indicating also a slower approach to final CA (though after some time evaporation takes place limiting the possibility to obtain an equilibrium CA). The stretched exponential form has been widely used in the past to describe complex relaxation, where more mechanisms contribute to a phenomenon.[35] By contrast, for the amorphous NPs, we obtained an almost simple exponential increase $c \approx 1$ as the fit in Fig. 3(b) indicates. This type of exponential for cos(CA) suggests that the NPs on the sample surface have a surfactant-like behaviour[41,42] that determines the droplet spreading towards a relaxed state.

Using the measured CA, we also obtained an estimation of the size of the drop, as the CA decreases to its final state, via the expression[41,42] $r_D = (6V/\pi)^{1/3}[\tan(CA/2)(3 + \tan^2(CA/2))]^{-1/3}$, where r_D is the radius of the wetted spot and V is the drop volume (prior to water evaporation) that is assumed to remain constant. The inset in Fig. 3(a) indicates that the size of the drop to its almost final hydrophilic state increases by almost ~100%. The more rapid increase in r_D occurs within ~2 to 3 s, while after this short transient it follows a slow increase as a power law with $r_D/(6V/\pi)^{1/3} \approx 0.7t^{0.1}$. In contrast, for the amorphous NPs (inset Fig. 3(b)), we only observe a weak increment of r_D up to ~10% in agreement with the strong droplet pinning on the surface. Moreover, if we introduce the dimensionless wetted area $S(t) = r_D^2/(6V/\pi)^{2/3}$ and substitute $Y = \cos(CA)$, we obtain $S(t) = (1 + Y)(1 - Y)^{-3}(4 + 2Y)^{-2/3}$.[42] S(t) also shows a stretched exponential temporal dependence $S(t) \sim [1 - \exp(-(bt)^c)]$ with an exponent $c \approx 0.54$ (see in supplementary material Fig. 7S) that is close to that obtained for cos(CA), despite the more complex dependence on cos(CA). In addition, the spreading rate is positive with $dS(t)/dt > 0$, but it decreases with time since $d^2S(t)/dt^2 < 0$ (see in supplementary material the inset of Fig. 6S) corresponding to a behaviour also known as "low surfactant activity,"[42] if we consider the effect of the crystallized GST as a type of surfactant.

Despite the strong differences in wetting behaviour for the amorphous and crystalline states of the GST NPs, the water drops remain firmly attached on the surface (after tests we performed at 90° inclinations and fully inverted; also, the receding/advancing CA was close to the static CA), indicating the formation of a rose petal or equivalently a Wenzel like state, where liquid is wetting surface crevices at least in the outer area of the droplets to yield strong sufficient surface pinning in a manner similar to the Cu NPs.[27] This is also supported by the accumulation of more material along the periphery of the water drop, as the SEM images indicate (see in supplementary material Fig. 3S) forming a boundary of height ~300 to 400 nm that is much larger than the average NP size ~20 nm.[32] The accumulation of NPs at the boundary is more pronounced for the crystallized GST samples, where

it appears that some fusion of the NPs has taken place during thermal annealing. The strong pinning of water droplets for the amorphous NPs is attributed to strong capillary forces within the nanoporous structure of the NP assemblies decorating the surfaces.[27] However, for the crystallized GST, the partial reduction in porosity leads to increased hydrophilicity though the pinning of the triple line still remains significant to sustain a rose petal behaviour. Note that the Wenzel model predicts that the roughness will enhance the hydrophilic/hydrophobic nature of surfaces. Since the bare HOPG surface has a wetting angle $<90°$, it is expected that the addition of NPs, leading to surface roughness, decreases CA or equivalently increases hydrophilicity. This clearly holds for the crystalline state, while it is reversed for the amorphous NPs due to the higher porosity leading to stronger pinning and thus higher CA.

Finally, we tested the wetting nature of the GST NP surfaces by measuring the capillary adhesion force due to water meniscus formation upon contact with another surface (at effective separations for spontaneous meniscus formation <3 nm).[43–46] The capillary force measurements were performed with the AFM using a micron size smooth borosilicate sphere (20 μm in diameter and hydrophilic)[46] attached on a tipless cantilever (sphere-plate geometry) and a softer tipless cantilever to compare the effect from different interaction geometries (and thus surface interaction areas), as it is shown in Fig. 4. For consistency, we tested the sphere on a flat SiC surface yielding large adhesion forces in agreement with the past studies.[45,46] The force measurements were averaged over 10 consecutive repetitions, and the maximum measured force is shown for both the amorphous and crystalline GST surfaces. In both cases, the adhesion force is stronger for the crystallized GST surface in agreement with its increased hydrophilic nature. However, for the amorphous NPs, the increased contact angle due to pinning (leading to increased hydrophobic behaviour) leads apparently to weaker capillary forces implying thinner water surface layer,[45,46] though by itself the surface of amorphous GST NPs is hydrophilic. Also, with increasing GST surface roughness (if we compare in Fig. 4 the samples HOPG-7 and 8), the capillary force strongly diminishes. This is because only a few surface asperities contribute to the force[44,45] or say even a single NP at the apex position leading to adhesion forces of the order of $\sim$10 nN, with the amorphous/crystalline surfaces showing the same trend. Quantitative understanding of capillary forces on NP assemblies is also complicated by the fact that in many instances the surface probe (e.g., sphere, tipless cantilever, etc.) picks up NPs leading to weak capillary forces.

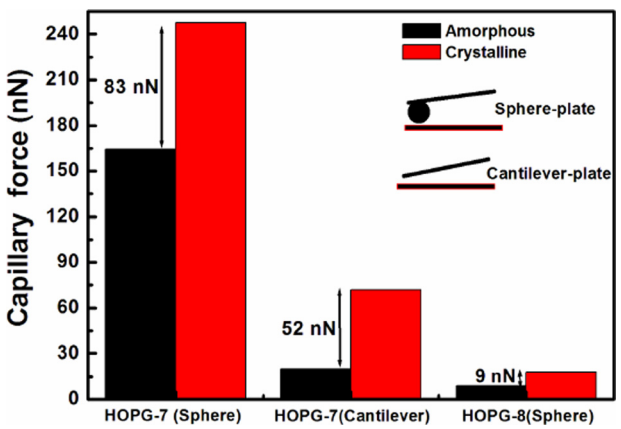

FIG. 4. Capillary adhesion force measurements with an AFM using a 20 μm in diameter borosilicate sphere attached on a cantilever with spring constant k = 2.25 N/m and directly with a tipless cantilever of spring constant k = 0.4 N/m. The latter was less stiff in order to increase the force sensitivity since in this case the interaction area, and the formation of the capillary meniscus was smaller than that of the sphere. The HOPG 7 and 8 indices indicate different samples with the 8-series being rougher leading to weaker adhesion.

In conclusion, our study demonstrated, as a *proof-of-concept*, that surface wetting can be physically changed between highly hydrophobic and hydrophilic states using the amorphous-to-crystalline phase transitions of GST NPs as a kind of surfactant. The CA measurements have shown that by increasing the coverage of amorphous NPs the contact angle increases to values close to the superhydrophobic limit (for NP coverages $\geq$80%), while for the crystallized GST the CA decreases down to $\sim$40° indicating significant hydrophilicity. Moreover, the GST phase also affects capillary adhesion due to water meniscus formation by being stronger for the more hydrophilic crystallized GST state. Therefore, the PCM NPs offer a potent strategy to tune surface wetting depending on the desired application.

See supplementary material for the NP deposition system, SEM, TEM, AFM analysis, and plots related to droplet kinetics.

We would like to acknowledge support by the Zernike Institute for Advanced Materials, University of Groningen Netherlands.

[1]P. G. de Gennes, Rev. Mod. Phys. **57**, 827 (1985).
[2]D. Bonn, J. Eggers, J. Indekeu, J. Meunier, and E. Rolley, Rev. Mod. Phys. **81**, 739 (2009).
[3]G. I. Loeb and M. E. Schrader, *Modern Approaches to Wettability: Theory and Applications* (Springer, 1992).
[4]V. M. Starov, M. G. Velarde, and C. J. Radke, *Wettability* (CRC, Boca Raton, 2007).
[5]S. Anand, A. T. Paxson, R. Dhiman, J. D. Smith, and K. K. Varanasi, ACS Nano **6**, 10122 (2012).
[6]X. Chen, J. Wu, R. Ma, M. Hua, N. Koratkar, S. Yao, and Z. Wang, Adv. Funct. Mater. **21**, 4617 (2011).
[7]C.-H. Chen, Q. Cai, C. Tsai, C.-L. Chen, G. Xiong, Y. Yu, and Z. Ren, Appl. Phys. Lett. **90**, 173108 (2007).
[8]D. 't Mannetje, S. Ghosh, R. Lagraauw, S. Otten, A. Pit, C. Berendsen, J. Zeegers, D. van den Ende, and F. Mugele, Nat. Commun. **5**, 3559 (2014).
[9]A. Tricoli, M. Righettoni, and S. E. Pratsinis, Langmuir **25**, 12578 (2009).
[10]C. Neinhuis and W. Barthlott, Ann. Bot. **79**, 667 (1997).
[11]W. Barthlott and C. Neinhuis, Planta **202**, 1 (1997).
[12]M. Callies and D. Quere, Soft Matter **1**, 55 (2005).
[13]D. Quéré, Physica A **313**, 32 (2002).
[14]G. Palasantzas, J. Th. M. DeHosson, K. F. L. Michielsen, and D. G. Stavenga, "Biomaterials," in *Handbook of Nanostructured Biomaterials and their Applications in Biotechnology* (American Scientific Publishers, 2005), Vol. 1.
[15]D. G. Stavenga, S. Foletti, G. Palasantzas, and K. Arikawa, Proc. R. Soc. B **273**, 661 (2006).
[16]R. N. Wenzel, Ind. Eng. Chem. **28**, 988 (1936).
[17]A. B. D. Cassie and S. Baxter, Trans. Faraday Soc. **40**, 546 (1944).
[18]C. Ishino and K. Okumura, Eur. Phys. J. E **25**, 415 (2008).
[19]B. Bhushan and M. Nosonovsky, Philos. Trans. R. Soc. A **368**, 4713 (2010).
[20]L. Cao, H.-H. Hu, and D. Gao, Langmuir **23**, 4310 (2007).
[21]Y.-T. Cheng and D. Rodak, Appl. Phys. Lett. **86**, 144101 (2005).

[22]A. Checco, B. M. Ocko, A. Rahman, C. T. Black, M. Tasinkevych, A. Giacomello, and S. Dietrich, Phys. Rev. Lett. **112**, 216101 (2014).
[23]L. Cao, T. P. Price, M. Weiss, and D. Gao, Langmuir **24**, 1640 (2008).
[24]A. Tuteja, W. Choi, J. M. Mabry, G. H. McKinley, and R. Cohen, Proc. Natl. Acad. Sci. **105**, 18200 (2008).
[25]Z. He, M. Ma, X. Xu, J. Wang, F. Chen, H. Deng, K. Wang, Q. Zhang, and Q. Fu, Appl. Surf. Sci. **258**, 2544 (2012).
[26]A. Marmur, Langmuir **24**, 7573 (2008).
[27]G. H. ten Brink, N. Foley, D. Zwaan, B. J. Kooi, and G. Palasantzas, RSC Adv. **5**, 28696 (2015).
[28]M. Wuttig and N. YaMada, Nat. Mater. **6**, 824 (2007).
[29]E. R. Meinders, A. V. Mijritskii, L. van Pieterson, and M. A. Wuttig, *Optical Data Storage: Phase-Change Media and Recording* (Springer, Berlin, 2006).
[30]G. Torricelli, P. J. van Zwol, O. Shpak, C. Binns, G. Palasantzas, B. J. Kooi, V. B. Svetovoy, and M. Wuttig, Phys. Rev. A **82**, 010101(R) (2010).
[31]G. Torricelli, P. J. van Zwol, O. Shpak, G. Palasantzas, V. B. Svetovoy, C. Binns, B. J. Kooi, P. Jost, and M. Wuttig, Adv. Funct. Mater. **22**, 3729 (2012).
[32]B. Chen, G. H. ten Brink, G. Palasantzas, and B. J. Kooi (submitted).
[33]G. H. Brink, G. Krishnan, B. J. Kooi, and G. Palasantzas, Appl. Phys. **116**, 104302 (2014).
[34]See www.mantisdeposition.com for the NP deposition system.
[35]J. Krim and G. Palasantzas, Int. J. Mod. Phys. B **9**, 599 (1995).
[36]G. Palasantzas, Phys. Rev. E **56**, 1254 (1997).
[37]V. B. Svetovoy and G. Palasantzas, Adv. Colloid Interface Sci. **216**, 1 (2015).
[38]M. Sedighi, V. B. Svetovoy, W. H. Broer, and G. Palasantzas, Phys. Rev. B **89**, 195440 (2014).
[39]See http://www.surface-tension.org/news/54.html for Young-Laplace equation fitting method (ADSA-PTM): Using the complete drop shape for measurement of static contact angle.
[40]Z. Xu, IET Micro Nano Lett. **9**, 6 (2014).
[41]V. M. Starov, S. R. Kosvintsev, and M. G. J.Velarde, Colloid Interface Sci. **227**, 185 (2000).
[42]K. S. Lee, N. Ivanova, V. M. Starov, N. Hilal, and V. Dutschk, Adv. Colloid Interface Sci. **144**, 54 (2008).
[43]H. J. Butt, B. Cappella, and M. Kappl, Surf. Sci. Rep. **59**, 1 (2005).
[44]J. Israelachvili, *Intermolecular and Surface Forces*, 3rd ed. (Elsevier Science Publishing, 2011).
[45]P. J. van Zwol, G. Palasantzas, and J. Th. M. de Hosson, Phys. Rev. E **78**, 031606 (2008).
[46]M. Sedighi, V. B. Svetovoy, and G. Palasantzas, Phys. Rev. E **93**, 062803 (2016).